Structure
Short Article

Open-Channel Structures of the Human Glycine Receptor α1 Full-Length Transmembrane Domain

David D. Mowrey,[3,5] Tanxing Cui,[1,5] Yuanyuan Jia,[1] Dejian Ma,[1] Alexander M. Makhov,[4] Peijun Zhang,[4] Pei Tang,[1,2,3,*] and Yan Xu[1,2,4,*]
[1]Department of Anesthesiology
[2]Department of Pharmacology and Chemical Biology
[3]Department of Computational and Systems Biology
[4]Department of Structural Biology
University of Pittsburgh School of Medicine, Pittsburgh, PA 15260, USA
[5]These authors contributed equally to this work and are co-first authors.
*Correspondence: tangp@upmc.edu (P.T.), xuy@anes.upmc.edu (Y.X.)
http://dx.doi.org/10.1016/j.str.2013.07.014

SUMMARY

Glycine receptors play a major role in mediating fast inhibitory neurotransmission in the spinal cord and brain stem, yet their high-resolution structures remain unsolved. We determined open-channel structures of the full-length transmembrane domain (TMD) of the human glycine receptor α1-subunit (hGlyR-α1) using nuclear magnetic resonance (NMR) spectroscopy and electron micrographs. hGlyR-α1 TMD spontaneously forms pentameric Cl^--conducting channels, with structures sharing overall topology observed in crystal structures of homologous bacterial and nematode pentameric ligand-gated ion channels (pLGICs). However, the mammalian hGlyR-α1 structures present several distinctive features, including a shorter, pore-lining TM2 helix with helical unwinding near the C-terminal end, a TM3 helical kink at A288 that partially overlaps with the homologous ivermectin-binding site in GluCl, and a highly dynamic segment between S267(15′) of TM2 and A288 that likely affects allosteric modulations of channel function. Our structures provide additional templates for identifying potential drug targets in GlyRs and other mammalian pLGICs.

INTRODUCTION

The glycine receptors are anion-selective channels and major inhibitory receptors in the human adult spinal cord and brain stem. They belong to the Cys-loop receptor superfamily, which also includes nicotinic acetylcholine receptors (nAChRs), type A and type C γ-amino-butyric acid ($GABA_A$ and $GABA_{A-\rho}$, respectively) receptors, and 5-hydroxytryptamine type 3 ($5\text{-}HT_3$) receptors. These membrane-embedded proteins mediate fast synaptic transmission in the peripheral and central nervous systems. They form pentameric ligand-gated ion channels (pLGICs) from five identical or homologous subunits. Each subunit contains an extracellular domain (ECD), a transmembrane domain (TMD), and an intracellular domain (ICD). ICD is involved in trafficking, localization, and modulation by secondary messengers but is not essential for the ion-transport function of the channel (Jansen et al., 2008). Upon agonist binding to the ECD, the channels open transiently to allow selected ions to permeate through the membrane, causing a change in the cross-membrane potential (Betz and Laube, 2006; Pless and Lynch, 2008).

Currently available structures for the Cys-loop receptors include the 4-Å cryo-electron microscopy (cryo-EM) model of the muscle-type nAChR (Unwin, 2005), nuclear magnetic resonance (NMR) structures of the TMD of the α4β2 nAChR (Bondarenko et al., 2012), and crystal structures of the α-bungarotoxin-bound α1 nAChR ECD (Dellisanti et al., 2007) and of a chimera from the acetylcholine binding protein (AChBP) and the α7 nAChR (Li et al., 2011). Crystal structures have also been solved for two prokaryotic homologs of Cys-loop receptors from the bacterium *Erwinia chrysanthemi* (ELIC) and cyanobacterium *Gloebacter violaceus* (GLIC) ligand-gated ion channels (LGICs) (Bocquet et al., 2009; Hilf and Dutzler, 2008, 2009) and for the ivermectin-bound nematode glutamate-gated chloride channel (GluCl) (Hibbs and Gouaux, 2011). Although these structures have greatly advanced the molecular understanding of Cys-loop receptors, no experimental structure is currently available for the TMD of any mammalian Cys-loop anion channels in an unliganded form.

The functional states of crystal structures are usually inferred from electrophysiology measurements under comparable conditions. The GluCl and GLIC structures are believed to represent either an open or desensitized conformation, whereas ELIC structures are thought to be in the closed conformation. Several hypothetical gating mechanisms have been proposed based on these structures (Corringer et al., 2010; Hibbs and Gouaux, 2011). However, it was recently discovered that crystallization conditions might bias the crystal structures into conformations that contradict electrophysiology results. A competitive antagonist-bound ELIC structure was found at the verge of channel opening (Pan et al., 2012b), yet the crystal structure of the mutation-stabilized open-channel ELIC is nearly identical to that of the closed ELIC (Gonzalez-Gutierrez et al., 2012). Anesthetic propofol inhibits GLIC current, but the crystal structure of the GLIC-propofol complex shows the same open-channel conformation as that observed in GLIC (Nury et al., 2011). These complications

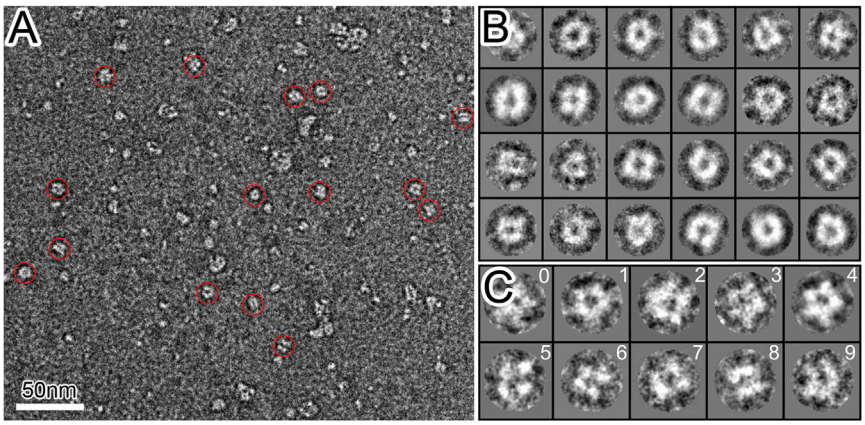

Figure 1. EM Analyses of the hGlyR-α1 TMD Oligomeric Complexes

(A) A raw electron micrograph of negatively stained hGlyR-α1 TMD oligomers in LPPG. Scale bar, 50 nm. Representative particles are indicated with red circles.

(B) Selected 2D class averages of hGlyR-α1 TMD oligomers from 210 particle images. Class averages show doughnut-shaped particles with a central channel and several oligomeric states, including pentamer and tetramer.

(C) Representative raw particle images corresponding to the pentameric (0–3) and tetrameric (5–7) configurations. An average of the raw particles from panels 0–3 is shown in panel 4. Panels 8 and 9 show side views of the particles.

See also Figure S2.

highlight the limitation of crystal structures in revealing functional states of Cys-loop receptors and the need for complementary structural approaches.

Recent advances in high-field NMR spectroscopy have made it possible to determine polytopic helical transmembrane (TM) structures for proteins ranging from an integral membrane enzyme to the phototaxis receptor sensory rhodopsin, and to various ion channels (Bondarenko et al., 2012; Gautier et al., 2010; Pielak et al., 2011; Van Horn et al., 2009; Verardi et al., 2011). Proteins examined in micelles and lipid bilayers often show similar structures, at least at the tertiary level (Gautier et al., 2010; Verardi et al., 2011). Lysophospholipids have been found particularly suitable for yielding good quality NMR spectra and retaining protein functionalities (Koehler et al., 2010; Krueger-Koplin et al., 2004). We report here the NMR structures of the full-length TMD of the human glycine receptor α1 subunit (hGlyR-α1), determined in the lysophospholipid lyso-1-palmitoylphosphotidylglycerol (LPPG). Electron microscopy (EM) and functional measurements show that the TMD forms pentameric and spontaneously Cl^--conducting channels. The NMR data revealed structural and dynamic features of the hGlyR-α1 TMD that may be shared by other anion-selective Cys-loop receptors. The functional relevance of the TMD structures is validated in a recent study (Duret et al., 2011), which found that the hGlyR-α1 TMD, in a chimera with the GLIC ECD, functions as an anion-selective channel and mirrors the pharmacological profile of the authentic hGlyR-α1.

RESULTS

The hGlyR-α1 TMD Forms Spontaneously Open Cl^- Channels

A protein encompassing the entire sequence (Figure S1 available online) of the hGlyR-α1 TMD was expressed and reconstituted in LPPG lipid micelles for structure determination using EM and high-resolution NMR. Unlike the GlyR ECD that assembles randomly into dimers and higher order oligomers (Haeger et al., 2010), the full-length hGlyR-α1 TMD spontaneously assembles into pentameric structures in LPPG lipid micelles. The negatively stained EM images (Figure 1) show face-on projections of pentamers. A small population of tetramers is also discernible, in accordance with the tetrameric subconductance state measurable in the authentic GlyR from mouse spinal cord neurons (Twyman and Macdonald, 1991). Circular averaging of all face-on pentamer images yielded a ring diameter of ~45 Å for the peak intensities (Figure S2), corresponding to a distance of ~26 Å between electron density centers of two adjacent subunits and ~43 Å between two nonadjacent subunits.

We also reconstituted the same expressed protein into large unilamellar vesicles (LUV) made of L-α phosphatidylcholine (PC) and phosphatidylglycerol (PG) lipids. Function of the hGlyR-α1 TMD channel for Cl^- transport was measured by NMR magnetization-inversion transfer (MIT) experiments (Hinton et al., 1994; Tang et al., 1999) using $Co(Gly)_3^-$ as a Cl^- shift reagent (Diven et al., 2003) to separate intra- and extravesicle ^{35}Cl resonances. We found that the channels are not only spontaneously open in the absence of the agonist-binding ECD but also Cl^- permeable (Figure 2A). At a nominal channel density of ~20–2,000 per vesicle, the unidirectional Cl^- efflux and influx rates (Tang et al., 1999) are 1,350 ± 460 and 560 ± 290 s^{-1}, respectively. Moreover, the Cl^- transport across the TM channels can be completely blocked in the presence of 1 mM picrotoxin (Figure 2B), indicating that the quaternary association of the TMD is preserved to form a functional channel with a pore geometry resembling that of the authentic open channel.

NMR Structure of the hGlyR-α1 TMD

A bundle of 15 monomer structures of the hGlyR-α1 TMD with the lowest target function from the CYANA calculation (Figure 3) exhibits a typical four-helix-bundle fold, which has been observed in the TMD structures of the α4β2 nAChR (Bondarenko et al., 2012) and other known structures of pLGICs (Bocquet et al., 2009; Hilf and Dutzler, 2008; Pan et al., 2012a, 2012b). The tertiary (Figure 3A) and quaternary (Figure 3B) packing of the TM helices were determined from the long-range intrasubunit and interhelical nuclear Overhauser effect (NOE) connectivity (Figures S3 and S4), paramagnetic relaxation enhancement (PRE) restraints (Battiste and Wagner, 2000) (Figure S5), and diameter restraints derived from the EM images. The orientation of the TM2 helix relative to the membrane normal was determined using the residual dipole coupling data from the TM2-TM3 helical segments in low-q bicelles as reported elsewhere (Canlas et al., 2008; Supplemental Experimental Procedures). The NMR structure statistics for the bundles of 15 monomers (Protein Data Bank [PDB] code: 2M6B) and 15 pentamers (PDB code: 2M6I) are

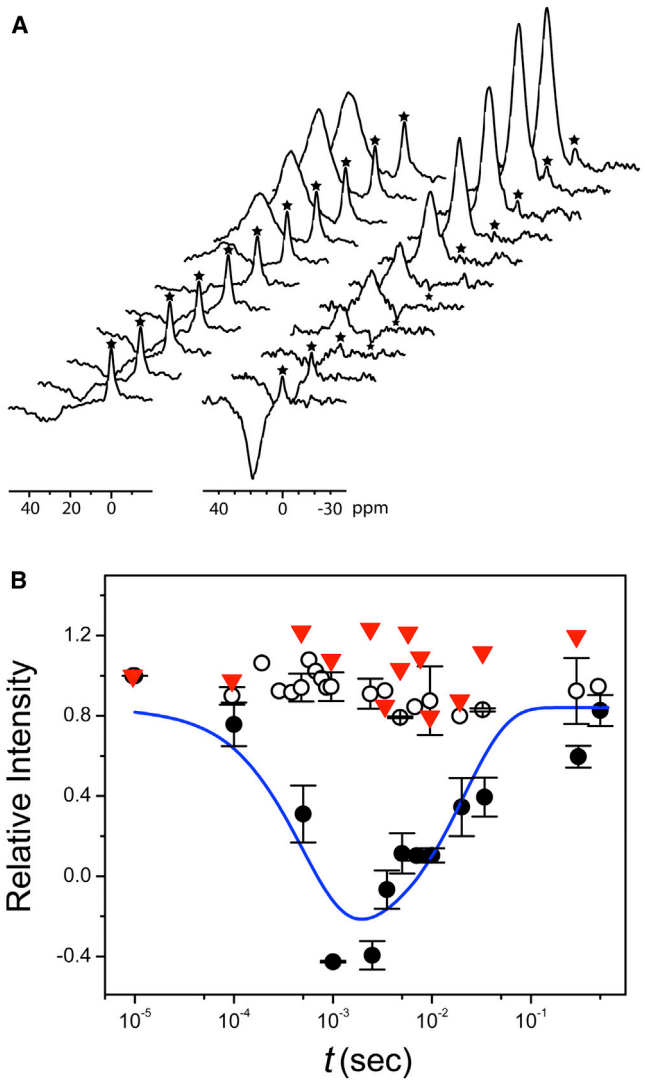

Figure 2. Channel Functional Measurements

(A) Stack plots of ^{35}Cl NMR spectra in Cl^- flux measurements across LUV by NMR MIT experiments (see Supplemental Experimental Procedures for experimental details). Left: control vesicles without the protein; Right: vesicles with hGlyR-α1 TMD channels. The Cl^- shift reagent $Co(Gly)_3^-$ separates the extravesicle Cl^- signal from the intravesicle signal (indicated by asterisks). The intensity of the intravesicle signal (*) changes as a function of the inversion-recovery time (t) due to the exchange of intra- and extravesicle Cl^-.

(B) The rates of Cl^- influx (k_i) and efflux (k_e) are determined by fitting the intensity changes as a function of t with a two-site exchange model (solid line, see fitting details in Supplemental Experimental Procedures). ○, LUV without protein; ●, LUV with protein; ▼, LUV with the same amount of protein and with 1 mM picrotoxin. Error bars show the SEM.

summarized in Table 1. The pairwise root-mean-square deviations (rmsd) among the 15 lowest target-function pentamer structures are 0.50 Å and 0.91 Å for the backbone and all heavy atoms, respectively, in the four membrane-spanning helices. The overall helical content calculated from the bundle of the NMR structures is 58%–62%, in excellent agreement with the value (58%) determined by the circular dichroism (CD) of hGlyR-α1 in LPPG.

Several structural features of the hGlyR-α1 TMD are worth noting. First, the pore-lining TM2 has a stable α-helix involving residues from P250 (−2′) to S267 (15′). Residues from 16′ to 18′ show an unwound helix exhibiting a slightly larger helical pitch (Figure 3A). The residues after 18′ in TM2 are nonhelical. In contrast, structures of several pLGICs, including the α4β2 nAChR determined by NMR (Bondarenko et al., 2012), show a longer TM2 α-helix that typically contains 23 residues (−2′ to 20′).

Second, unlike a straight helix observed in other pLGICs, the TM3 helix of hGlyR-α1 has a kink at A288 (Figure 3A). The kink changes the helix axis direction by ~33°. It is also notable that the fourth residue upstream from the kink is a conserved aspartate (D284). Aspartate is known to frequently locate at the i–4 position of TM helical bends (Langelaan et al., 2010).

Third, while most of the pore-lining residues in the hGlyR-α1 TMD structure (Figure 3C) agree well with homologous residues in the previously published pLGIC structures, one distinction is that the well-conserved L261 (9′) in our open-channel structures does not directly face the lumen of the pore, but T262 (10′) does.

Finally, the open channel pore of hGlyR-α1 has a cone shape, with the smallest diameter of 6.2 Å at a hydrophobic girdle defined by P250 (−2′) and A251 (−1′) side chains situated at the cytoplasmic side of the membrane (Figure 3D). The positively charged R252 (0′) side chains are tangential to the circumference of the pore. The constriction size of the hGlyR-α1 open pore is close to the estimated 6.2 Å for glycine and $GABA_A$ receptors based on the studies of ion permeability (Fatima-Shad and Barry, 1993).

Dynamics of the hGlyR-α1 TMD

The dynamic characteristics of the TM2 and TM3 helices near the TM2-3 loop are observed not only in the bundle of structures (Figure 3A) but also directly in the high-resolution NMR spectra, where two sets of NMR peaks are identifiable for several residues near the TM2 C terminus, including S268 (16′), G269 (17′), and S270 (18′) (Figure 4A). The data suggest that at least two conformations coexist in this region and that they undergo slow exchange on the microsecond timescale used for NMR data acquisition. It should be noted that a similar minor conformation was also observed in an extended TM2 segment of GlyR (Yushmanov et al., 2003) and in the TM2-TM3 construct in lipid bicelles (Canlas et al., 2008). The NMR structures determined in the present study are associated with the major peaks. The structure in the minor conformation could not be determined because of insufficient NOE spectroscopy (NOESY) connectivity. A considerable degree of conformational flexibility in the region of the TM2 and TM3 helices near the TM2-3 loop is also evident in the backbone dynamics (Figure S6), as measured by the ^{15}N relaxation parameters (R_1 and R_2) and ^{15}N-{^1H} heteronuclear NOE (hetNOE) of the major peaks. Nearly 60% of the hGlyR-α1 residues result in relatively high hetNOE values, in agreement with the helical contents determined by CD, the chemical shift index, and the final structures. However, the segment from S267 (S15′) in TM2 to K276 (K24′) in the TM2-3 loop, and residues involved in the TM3 helical kink, such as W286, show smaller hetNOE and R_2 values and relatively higher R_1, suggesting high flexibility in the region.

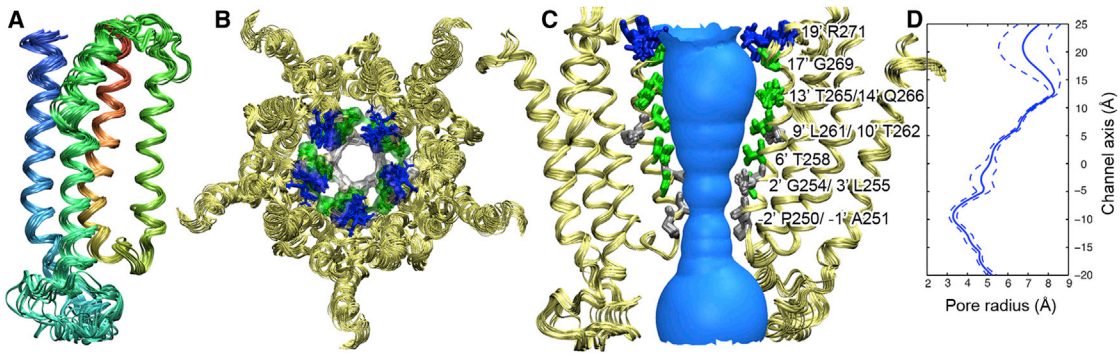

Figure 3. NMR Structures of the hGlyR-α1 TMD

(A) A bundle of 15 lowest target function monomer structures of the hGlyR-α1 TMD (PDB code: 2M6B). The TM1, TM2, TM3, and TM4 helices are indicated in red, light green, green, and blue, respectively.

(B) Top view of a bundle of the 15 lowest target function pentameric structures of the hGlyR-α1 TMD (PDB code: 2M6I), calculated using CYANA with restraints generated from NMR and EM data. Pore lining residues are highlighted based on residue type: green, polar; gray, nonpolar; and blue, basic.

(C) Side view of the bundle of the15 lowest target function pentameric structures of the hGlyR-α1 TMD. For clarity, only two subunits are shown. Pore lining residues are labeled and colored based on their residue type.

(D) The pore profile calculated using the HOLE program (Smart et al., 1996). Dashed lines represent ±1 SD determined from the bundle of 15 lowest target function structures.

See also Figures S3–S5.

DISCUSSION

It is remarkable that the hGlyR-α1 TMD alone, without the ICD or ECD, can self-assemble into a pentameric channel in the membrane-mimetic environment. It is perhaps even more remarkable that the assembled channels spontaneously conduct Cl^-. These results, along with the previous finding on well-assembled and spontaneously open channels of the α4β2 nAChR TMD (Bondarenko et al., 2012), support the notion that the ECD serves as a regulator that creates an energy barrier between open and closed states and constrains the TM channel to the closed state. In the presence of the ECD but without agonist binding, the closed-channel (nonconducting) conformation is preferred, and there is an energy barrier to the open state. In the absence of the ECD, however, either the open-channel (conducting) conformation has become preferred or the energy barrier between open- and closed-channel conformations has been relaxed to allow spontaneous channel opening. Our NMR spectra show that residues at the C-terminal end of TM2 exchange between two distinct conformations, possibly related to the open and closed states. The fact that NMR spectra can simultaneously capture two conformations in this region suggests that the free energy difference between the two conformations is not large.

The NMR-resolved structures of the hGlyR-α1 TMD show a general topological agreement with the pLGIC structures determined previously, but several notable differences may be functionally important. One distinct difference is the relatively short TM2 helix, which is about a half helical turn shorter than TM2 helices of ELIC (Hilf and Dutzler, 2008; Pan et al., 2012b), GLIC (Bocquet et al., 2009; Hilf and Dutzler, 2009; Pan et al., 2012a) and GluCl (Hibbs and Gouaux, 2011), but about two helical turns (seven residues) shorter than TM2 helices shown in the cryo-EM structure of nAChR (Unwin, 2005). One may wonder if a shorter TM2 helix is due to different methodologies, NMR versus X-ray. Our previously published NMR structures of the α4β2 nAChR TMD (Bondarenko et al., 2012) negate this possibility. Both α4 and β2 show a TM2 helical length similar to that observed in ELIC, GLIC, and GluCl. The discrepancy in the TM2 helical length between hGlyR-α1 and other pLGICs occurs at the C-terminal end of TM2, where the helix ends at the 18′ residue (with slight unwinding after 15′) in hGlyR-α1, but at 20′ in other pLGICs. Furthermore, the TM2 residues S268 (16′), G269 (17′), and S270 (18′) of hGlyR-α1 undergo slow exchange between two distinct conformations that have not been observed in the α4β2 nAChR using the same NMR method. These results demonstrate the unique structural flexibility at the extracellular (EC) end of the pore in hGlyR-α1. Compared to other pLGICs, glycine receptors are uniquely rich with serine residues (15′, 16′, 18′) near the TM2 C terminus (Figure S1). It is known that the OH group of serine can weaken the helical backbone hydrogen bonds by constraining the carbonyl oxygen through the O···H-O interaction (Ballesteros et al., 2000). The presence of a cluster of serines near the TM2 C terminus may have contributed to the structural flexibility in the region.

It is also notable in the bundle of NMR structures (Figure 3) that R271 (19′) shows conformational variation with a smaller population in a more extended helix and a larger population in an unwound conformation. Consequently, instead of facing the pore, R19′ in some structures is mostly tangent to the pore, where R271 (19′) experiences a more hydrophobic environment. Indeed, such conformational flexibility was noted previously by tethering a rhodamine fluorophore to R271C (Pless et al., 2007), in which the experiment showed a population shift of the fluorescence probe at 19′ to a more hydrophobic environment upon channel opening, suggesting that conformational flexibility at the EC end of the pore is related to channel function. Ester substitution is expected to weaken the backbone hydrogen bonds and increase the flexibility of the pore-lining TM2 helix. Single-point amide-to-ester mutations at 13′, 16′, or

Table 1. Summary of NMR Structure Statistics and Restraints for the hGlyR-α1 TM Domain in LPPG Micelles

NMR Distance and Dihedral Restraints and Structure Statistics	Monomer	Pentamer
Distance restraints		
Total NOE	1,014	1,014 × 5
Intraresidue	321	321 × 5
Interresidue	693	693 × 5
Sequential (|i − j| = 1)	348	348 × 5
Medium range (|i − j| ≤ 4)	324	324 × 5
Long range (|i − j| > 4)	21	21 × 5
Hydrogen bonds	106	106 × 5
Total dihedral angle restraints	152	154 × 5
Phi	76	77 × 5
Psi	76	77 × 5
PRE restraints	219	226 × 5
Upper	107	114 × 5
Lower	112	112 × 5
Intersubunit distance restraints from EM and RDC[a]		
Total constraints		600
Upper		300
Lower		300
Structure statistics		
Violations (mean and SD)		
Upper distance restraints (Å)	0.0075 ± 0.0008	0.0157 ± 0.0010
Lower distance restraints (Å)	0.0016 ± 0.0010	0.0102 ± 0.0012
Dihedral angle restraints (°)	0.130 ± 0.010	0.338 ± 0.028
Maximum dihedral angle violation (°)	1.29	3.32
Maximum distance restraint violation (Å)	0.24	0.63
Average pairwise rmsd[b] (Å)		
Heavy	1.04 ± 0.11[c]	0.91 ± 0.14[c]
	2.27 ± 0.25[d]	1.50 ± 0.36[d]
Backbone	0.67 ± 0.13[c]	0.50 ± 0.17[c]
	1.66 ± 0.18[d]	0.95 ± 0.30[d]
Ramachandran plot (%)		
Residues in most favored regions	88.6	86.3
Residues in allowed regions	11.3	13.0
Residues in disallowed regions	0.1	0.7
PDB code	2M6B	2M6I

See also Figures S3–S5.
[a]RDC values used to generate pentamer restraints were obtained from the previous study (Canlas et al., 2008).
[b]The rmsd to the average coordinates was calculated from 15 structures.
[c]Calculated over the helical TM regions (residues 220–241, 250–270, 289–305, and 398–421).
[d]Calculated over residues 215–425.

19′ of nAChR increased the receptor's sensitivity to agonist more than 10-fold (England et al., 1999). A more recent study using electron paramagnetic resonance spectroscopy also observed greater conformational changes at the EC end of TM2 upon agonist binding (Velisetty et al., 2012).

The high flexibility of the TM2 C terminus of hGlyR-α1 is likely coupled with the structural flexibility near the N-terminal helix of TM3. A helical kink (I285–A288) divides the TM3 domain into two α-helical segments: one from V277 to D284 and the other from V289 to V307 (Figure 3A and Figure S3). Three points about the kink are worth noting. First, statistically speaking, D284 is likely responsible for the kink formation. Analysis of nonredundant polypeptide chains revealed kinks in 64% of TM helices, and aspartate showed a notably high frequency at the i–4 position of the TM helical kink (Langelaan et al., 2010), although it remains unclear why aspartate promotes the helical disruption. Second, D284 is conserved in both glycine and $GABA_A$ receptors. It likely plays a similar structural and functional role in all anion-conducting Cys-loop receptors. Mutation of this conserved aspartate in the α1 $GABA_A$ receptor significantly reduced receptor activity (Bera et al., 2002). Third, although the TM3 helices in the crystal structure of the GluCl and ivermectin complex show no kink (Hibbs and Gouaux, 2011), the kink may exist in the absence of ivermectin. When we aligned the TM structures of GluCl and hGlyR-α1, it became clear that ivermectin partially overlapped with the kink observed in the NMR structure (Figure 4B), suggesting that ivermectin binding may have stabilized a straight helical conformation and that without ivermectin, the flexibility would make it much more challenging to obtain high-quality GluCl crystals for X-ray structure determination.

S267 and A288 mark the two ends of a dynamic region of the channel in our hGlyR-α1 TMD structures (Figure 4C). It is intriguing that mutations S267Y and A288W in the hGlyR-α1 TMD were found to substantially reduce general anesthetic and alcohol potentiation of GlyR responses (Mihic et al., 1997). Mutations at S267 showed that ethanol modulation was correlated with the volume but not the polarity or hydropathicity of the substituting side chains, suggesting that S267 itself is not directly involved in alcohol binding (Ye et al., 1998). These functional consequences may result from the reduced conformational flexibility in the region due to bulky substitution at the S267 position. In fact, our previous NMR study demonstrated that the S267Y mutation increased the α-helix length at the TM2 C terminus (Tang et al., 2002). Mutation of A288 to an amino acid with a different size can also alter conformational flexibility in the region with functional consequences. Indeed, A288F and A288G have opposite functional impacts, with the former reducing and the latter increasing glycine-induced channel activation (Lynagh and Lynch, 2010). It is unlikely that glycine binding is affected by the mutations because the orthosteric agonist-binding site in the ECD is remote from A288. The changes in conformational flexibility due to mutations alter the channel's susceptibility to allosteric activation.

Q266H is a TM2 mutation that causes hyperekplexia (Moorhouse et al., 1999), a human genetic disease characterized by a startle response to acoustic or tactile stimulations. The mutation reduces the ability of glycine and taurine to activate the channel and reduces the channel open times, implicating a change in gating kinetics. Moreover, the mutation does not affect ion accessibility to the channel lumen (Moorhouse et al., 1999), consistent with the Q266 side chain orientation in the NMR

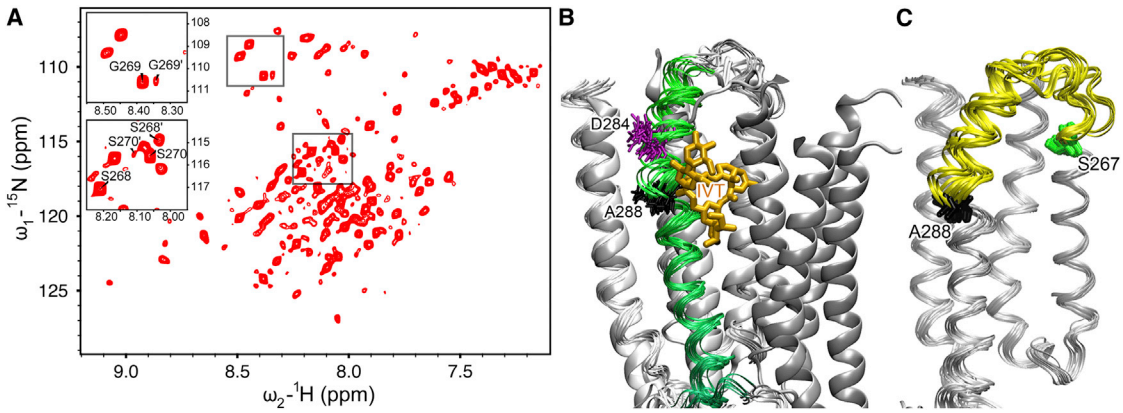

Figure 4. Conformational Dynamics around TM2-3 Loop

(A) A representative ^{1}H-^{15}N heteronuclear single-quantum coherence spectrum of the hGlyR-α1 TMD in LPPG micelles at 40°C. Several residues at the C terminus of TM2 show two sets of peaks, as exemplified in the insert for S268(16′), G269(17′), and S270(18′), indicating that two conformations coexist in this region and undergo slow conformational exchange.

(B) The 15 lowest target function structures of the hGlyR-α1 TMD (thin ribbons) are aligned with the crystal structure of GluCl (thick ribbon; PDB code: 3rhw). TM3 of the hGlyR-α1 TMD is highlighted in green. Ivermectin (IVT; orange sticks) observed in GluCl partially overlaps with the kink at A288 (black sticks) in the NMR structures of the hGlyR-α1 TMD. The residue D284 (purple sticks), located four residues upstream of A288, may be responsible for the kink (Langelaan et al., 2010).

(C) The segment showing high dynamics is highlighted in yellow between S267 (green) and A288 (black) in the bundle of the 15 lowest target function NMR structures.

See also Figure S6.

structure. It is interesting that Q266I also reduces glycine sensitivity and glycine-induced maximal currents (Borghese et al., 2012). Both H and I have a larger side chain than Q. Thus, Q266H and Q266I likely produce the same volume effects as in the S267 mutants, given the adjacency of Q266 and S267. Q has another unique property. The amide of its side chain can contact its own backbone carbonyl oxygen (Figure S7). This contact competes with helical hydrogen bonding, weakening the helical propensity and adding structural flexibility to the region. Self-contacts within glutamine have been observed in other proteins (Pal and Sankararamakrishnan, 2008).

The NMR structures of the GlyR-α1 TMD provide valuable structural and dynamic templates for the design and discovery of modulators or therapeutics targeting glycine receptors. For example, our TMD structure revealed a specific binding site in the GlyR-α1 TM3 domain for Δ^9-tetrahydrocannabinol (THC), the major ingredient of marijuana, and several other cannabinoids (Xiong et al., 2011, 2012). NMR chemical shift titration further showed the direct involvement of residue S296 in THC binding. Hydrogen-bond interaction of S296 with the hydroxyl groups of THC is considered to be critical for the THC potentiation of α1- and α3-containing GlyR in mediating THC's analgesic effects. This important drug-binding site would not be discovered from any homology modeling using the crystal structures of lower species. It is foreseeable that the structures of the GlyR-α1 TMD reported here will offer useful insights for other potential drugs targeting mammalian Cys-loop anion channels.

EXPERIMENTAL PROCEDURES

Detailed experimental procedures can be found in the Supplemental Experimental Procedures. Briefly, the full-length TMD of hGlyR-α1 was expressed and purified using the same methods as reported elsewhere (Ma et al., 2005). In addition to uniform ^{15}N-labeling and ^{15}N, ^{13}C-double labeling, specific ^{15}N labeling of alanine, phenylalanine, leucine, isoleucine, and valine were performed to assist in chemical shift assignment. Samples for high-resolution NMR were prepared in LPPG micelles having a protein concentration of ~500 μM with a protein-to-LPPG ratio of ~1:200 (pH 5.8). The choice of LPPG was made based on protein sample stability, high NMR spectral quality, and pentameric channel formation as shown in EM. For EM measurements, serial dilutions were made from a stock solution of 54 μM protein and a protein-to-LPPG ratio of 1:50. To generate long-range distance restraints by PRE, the wild-type hGlyR-α1 TM (with one cysteine, C290) and two single-cysteine mutants (C290S/S296C and C290S/S308C) were prepared and labeled with [1-oxyl-2,2,5,5-tetramethylpyrroline-3-methyl]-methanethiosulfonate. For functional Cl^- flux measurements, hGlyR-α1 was reconstituted into 3:1 PC:PG LUV for MIT experiments.

NMR experiments were carried out at 40°C on Bruker Avance 600, 700, 800, or 900 MHz spectrometers equipped with triple-resonance inverse-detection cryoprobes (Bruker Instruments, Billerica, MA, USA). A standard suite of two- and three-dimensional (2D and 3D, respectively) pulse sequences was used for resonance assignment, structure calculations, protein dynamics measurements, and Cl^- flux measurements, as detailed in the Supplemental Experimental Procedures. EM experiments were performed at 200 kV using a TF20 electron microscope (FEI, Hillsboro, OR, USA) equipped with a 4K × 4K Gatan CCD camera. CYANA 3.0 (López-Méndez and Güntert, 2006) was used for structure calculations with a combination of angular and distance restraints from chemical shift, 3D NOESY, PRE, EM, and residual dipolar coupling (RDC) measurements, as summarized in Table 1. The VMD program (Humphrey et al., 1996) was used for structure rendering, visualization, and analysis. The pore profiles were analyzed using the HOLE program (Smart et al., 1996).

ACCESSION NUMBERS

The Biological Magnetic Resonance Bank accession number for the NMR chemical shift assignments reported in this article is 19126. The PDB codes for the monomeric and pentameric structures reported in this article are 2M6B and 2M6I, respectively.

SUPPLEMENTAL INFORMATION

Supplemental information includes Supplemental Experimental Procedures, seven figures, and one table and can be found with this article online at http://dx.doi.org/10.1016/j.str.2013.07.014.

ACKNOWLEDGMENTS

The authors thank Ling Li for technical assistance with protein expression, Professor Peter Güntert for providing a prereleased version of CYANA 3.0 for pentamer structure calculation, and Sandra C. Hirsch for editorial assistance. This work was supported by grants from the National Institutes of Health (R37GM049202, R01GM056257, R01GM069766, and R01 GM085043).

Received: April 4, 2013
Revised: June 19, 2013
Accepted: July 22, 2013
Published: August 29, 2013

REFERENCES

Ballesteros, J.A., Deupi, X., Olivella, M., Haaksma, E.E.J., and Pardo, L. (2000). Serine and threonine residues bend alpha-helices in the chi(1) = g(-) conformation. Biophys. J. *79*, 2754–2760.

Battiste, J.L., and Wagner, G. (2000). Utilization of site-directed spin labeling and high-resolution heteronuclear nuclear magnetic resonance for global fold determination of large proteins with limited nuclear overhauser effect data. Biochemistry *39*, 5355–5365.

Bera, A.K., Chatav, M., and Akabas, M.H. (2002). GABA(A) receptor M2-M3 loop secondary structure and changes in accessibility during channel gating. J. Biol. Chem. *277*, 43002–43010.

Betz, H., and Laube, B. (2006). Glycine receptors: recent insights into their structural organization and functional diversity. J. Neurochem. *97*, 1600–1610.

Bocquet, N., Nury, H., Baaden, M., Le Poupon, C., Changeux, J.P., Delarue, M., and Corringer, P.J. (2009). X-ray structure of a pentameric ligand-gated ion channel in an apparently open conformation. Nature *457*, 111–114.

Bondarenko, V., Mowrey, D., Tillman, T., Cui, T., Liu, L.T., Xu, Y., and Tang, P. (2012). NMR structures of the transmembrane domains of the α4β2 nAChR. Biochim. Biophys. Acta *1818*, 1261–1268.

Borghese, C.M., Xiong, W., Oh, S.I., Ho, A., Mihic, S.J., Zhang, L., Lovinger, D.M., Homanics, G.E., Eger, E.I., 2nd, and Harris, R.A. (2012). Mutations M287L and Q266I in the glycine receptor α1 subunit change sensitivity to volatile anesthetics in oocytes and neurons, but not the minimal alveolar concentration in knockin mice. Anesthesiology *117*, 765–771.

Canlas, C.G., Ma, D., Tang, P., and Xu, Y. (2008). Residual dipolar coupling measurements of transmembrane proteins using aligned low-q bicelles and high-resolution magic angle spinning NMR spectroscopy. J. Am. Chem. Soc. *130*, 13294–13300.

Corringer, P.J., Baaden, M., Bocquet, N., Delarue, M., Dufresne, V., Nury, H., Prevost, M., and Van Renterghem, C. (2010). Atomic structure and dynamics of pentameric ligand-gated ion channels: new insight from bacterial homologues. J. Physiol. *588*, 565–572.

Dellisanti, C.D., Yao, Y., Stroud, J.C., Wang, Z.Z., and Chen, L. (2007). Crystal structure of the extracellular domain of nAChR alpha1 bound to alpha-bungarotoxin at 1.94 A resolution. Nat. Neurosci. *10*, 953–962.

Diven, C.F., Wang, F., Abukhdeir, A.M., Salah, W., Layden, B.T., Geraldes, C.F., and Mota de Freitas, D. (2003). Evaluation of [Co(gly)3]- as a 35Cl-NMR shift reagent for cellular studies. Inorg. Chem. *42*, 2774–2782.

Duret, G., Van Renterghem, C., Weng, Y., Prevost, M., Moraga-Cid, G., Huon, C., Sonner, J.M., and Corringer, P.J. (2011). Functional prokaryotic-eukaryotic chimera from the pentameric ligand-gated ion channel family. Proc. Natl. Acad. Sci. USA *108*, 12143–12148.

England, P.M., Zhang, Y., Dougherty, D.A., and Lester, H.A. (1999). Backbone mutations in transmembrane domains of a ligand-gated ion channel: implications for the mechanism of gating. Cell *96*, 89–98.

Fatima-Shad, K., and Barry, P.H. (1993). Anion permeation in GABA- and glycine-gated channels of mammalian cultured hippocampal neurons. Proc. Biol. Sci. *253*, 69–75.

Gautier, A., Mott, H.R., Bostock, M.J., Kirkpatrick, J.P., and Nietlispach, D. (2010). Structure determination of the seven-helix transmembrane receptor sensory rhodopsin II by solution NMR spectroscopy. Nat. Struct. Mol. Biol. *17*, 768–774.

Gonzalez-Gutierrez, G., Lukk, T., Agarwal, V., Papke, D., Nair, S.K., and Grosman, C. (2012). Mutations that stabilize the open state of the Erwinia chrisanthemi ligand-gated ion channel fail to change the conformation of the pore domain in crystals. Proc. Natl. Acad. Sci. USA *109*, 6331–6336.

Haeger, S., Kuzmin, D., Detro-Dassen, S., Lang, N., Kilb, M., Tsetlin, V., Betz, H., Laube, B., and Schmalzing, G. (2010). An intramembrane aromatic network determines pentameric assembly of Cys-loop receptors. Nat. Struct. Mol. Biol. *17*, 90–98.

Hibbs, R.E., and Gouaux, E. (2011). Principles of activation and permeation in an anion-selective Cys-loop receptor. Nature *474*, 54–60.

Hilf, R.J., and Dutzler, R. (2008). X-ray structure of a prokaryotic pentameric ligand-gated ion channel. Nature *452*, 375–379.

Hilf, R.J., and Dutzler, R. (2009). Structure of a potentially open state of a proton-activated pentameric ligand-gated ion channel. Nature *457*, 115–118.

Hinton, J.F., Newkirk, D.K., Fletcher, T.G., and Shungu, D.C. (1994). Application of the magnetization-inversion-transfer technique to the transport of 7Li+, 23Na+, and 39K+ ions through the gramicidin channel and the M2 delta transmembrane domain of the nicotinic acetylcholine receptor. J. Magn. Reson. B. *105*, 11–16.

Humphrey, W., Dalke, A., and Schulten, K. (1996). VMD: visual molecular dynamics. J. Mol. Graph. *14*, 33–38.

Jansen, M., Bali, M., and Akabas, M.H. (2008). Modular design of Cys-loop ligand-gated ion channels: functional 5-HT3 and GABA rho1 receptors lacking the large cytoplasmic M3M4 loop. J. Gen. Physiol. *131*, 137–146.

Koehler, J., Sulistijo, E.S., Sakakura, M., Kim, H.J., Ellis, C.D., and Sanders, C.R. (2010). Lysophospholipid micelles sustain the stability and catalytic activity of diacylglycerol kinase in the absence of lipids. Biochemistry *49*, 7089–7099.

Krueger-Koplin, R.D., Sorgen, P.L., Krueger-Koplin, S.T., Rivera-Torres, I.O., Cahill, S.M., Hicks, D.B., Grinius, L., Krulwich, T.A., and Girvin, M.E. (2004). An evaluation of detergents for NMR structural studies of membrane proteins. J. Biomol. NMR *28*, 43–57.

Langelaan, D.N., Wieczorek, M., Blouin, C., and Rainey, J.K. (2010). Improved helix and kink characterization in membrane proteins allows evaluation of kink sequence predictors. J. Chem. Inf. Model. *50*, 2213–2220.

Li, S.X., Huang, S., Bren, N., Noridomi, K., Dellisanti, C.D., Sine, S.M., and Chen, L. (2011). Ligand-binding domain of an α7-nicotinic receptor chimera and its complex with agonist. Nat. Neurosci. *14*, 1253–1259.

López-Méndez, B., and Güntert, P. (2006). Automated protein structure determination from NMR spectra. J. Am. Chem. Soc. *128*, 13112–13122.

Lynagh, T., and Lynch, J.W. (2010). A glycine residue essential for high ivermectin sensitivity in Cys-loop ion channel receptors. Int. J. Parasitol. *40*, 1477–1481.

Ma, D., Liu, Z., Li, L., Tang, P., and Xu, Y. (2005). Structure and dynamics of the second and third transmembrane domains of human glycine receptor. Biochemistry *44*, 8790–8800.

Mihic, S.J., Ye, Q., Wick, M.J., Koltchine, V.V., Krasowski, M.D., Finn, S.E., Mascia, M.P., Valenzuela, C.F., Hanson, K.K., Greenblatt, E.P., et al. (1997). Sites of alcohol and volatile anaesthetic action on GABA(A) and glycine receptors. Nature *389*, 385–389.

Moorhouse, A.J., Jacques, P., Barry, P.H., and Schofield, P.R. (1999). The startle disease mutation Q266H, in the second transmembrane domain of the human glycine receptor, impairs channel gating. Mol. Pharmacol. *55*, 386–395.

Nury, H., Van Renterghem, C., Weng, Y., Tran, A., Baaden, M., Dufresne, V., Changeux, J.P., Sonner, J.M., Delarue, M., and Corringer, P.J. (2011). X-ray

structures of general anaesthetics bound to a pentameric ligand-gated ion channel. Nature *469*, 428–431.

Pal, T.K., and Sankararamakrishnan, R. (2008). Self-contacts in Asx and Glx residues of high-resolution protein structures: role of local environment and tertiary interactions. J. Mol. Graph. Model. *27*, 20–33.

Pan, J., Chen, Q., Willenbring, D., Mowrey, D., Kong, X.P., Cohen, A., Divito, C.B., Xu, Y., and Tang, P. (2012a). Structure of the pentameric ligand-gated ion channel GLIC bound with anesthetic ketamine. Structure *20*, 1463–1469.

Pan, J., Chen, Q., Willenbring, D., Yoshida, K., Tillman, T., Kashlan, O.B., Cohen, A., Kong, X.P., Xu, Y., and Tang, P. (2012b). Structure of the pentameric ligand-gated ion channel ELIC cocrystallized with its competitive antagonist acetylcholine. Nat. Commun. *3*, 714.

Pielak, R.M., Oxenoid, K., and Chou, J.J. (2011). Structural investigation of rimantadine inhibition of the AM2-BM2 chimera channel of influenza viruses. Structure *19*, 1655–1663.

Pless, S.A., and Lynch, J.W. (2008). Illuminating the structure and function of Cys-loop receptors. Clin. Exp. Pharmacol. Physiol. *35*, 1137–1142.

Pless, S.A., Dibas, M.I., Lester, H.A., and Lynch, J.W. (2007). Conformational variability of the glycine receptor M2 domain in response to activation by different agonists. J. Biol. Chem. *282*, 36057–36067.

Smart, O.S., Neduvelil, J.G., Wang, X., Wallace, B.A., and Sansom, M.S. (1996). HOLE: a program for the analysis of the pore dimensions of ion channel structural models. J. Mol. Graph. *14*, 354–360, 376.

Tang, P., Hu, J., Liachenko, S., and Xu, Y. (1999). Distinctly different interactions of anesthetic and nonimmobilizer with transmembrane channel peptides. Biophys. J. *77*, 739–746.

Tang, P., Mandal, P.K., and Xu, Y. (2002). NMR structures of the second transmembrane domain of the human glycine receptor alpha(1) subunit: model of pore architecture and channel gating. Biophys. J. *83*, 252–262.

Twyman, R.E., and Macdonald, R.L. (1991). Kinetic properties of the glycine receptor main- and sub-conductance states of mouse spinal cord neurones in culture. J. Physiol. *435*, 303–331.

Unwin, N. (2005). Refined structure of the nicotinic acetylcholine receptor at 4A resolution. J. Mol. Biol. *346*, 967–989.

Van Horn, W.D., Kim, H.J., Ellis, C.D., Hadziselimovic, A., Sulistijo, E.S., Karra, M.D., Tian, C., Sönnichsen, F.D., and Sanders, C.R. (2009). Solution nuclear magnetic resonance structure of membrane-integral diacylglycerol kinase. Science *324*, 1726–1729.

Velisetty, P., Chalamalasetti, S.V., and Chakrapani, S. (2012). Conformational transitions underlying pore opening and desensitization in membrane-embedded Gloeobacter violaceus ligand-gated ion channel (GLIC). J. Biol. Chem. *287*, 36864–36872.

Verardi, R., Shi, L., Traaseth, N.J., Walsh, N., and Veglia, G. (2011). Structural topology of phospholamban pentamer in lipid bilayers by a hybrid solution and solid-state NMR method. Proc. Natl. Acad. Sci. USA *108*, 9101–9106.

Xiong, W., Cheng, K., Cui, T., Godlewski, G., Rice, K.C., Xu, Y., and Zhang, L. (2011). Cannabinoid potentiation of glycine receptors contributes to cannabis-induced analgesia. Nat. Chem. Biol. *7*, 296–303.

Xiong, W., Cui, T., Cheng, K., Yang, F., Chen, S.R., Willenbring, D., Guan, Y., Pan, H.L., Ren, K., Xu, Y., and Zhang, L. (2012). Cannabinoids suppress inflammatory and neuropathic pain by targeting α3 glycine receptors. J. Exp. Med. *209*, 1121–1134.

Ye, Q., Koltchine, V.V., Mihic, S.J., Mascia, M.P., Wick, M.J., Finn, S.E., Harrison, N.L., and Harris, R.A. (1998). Enhancement of glycine receptor function by ethanol is inversely correlated with molecular volume at position alpha267. J. Biol. Chem. *273*, 3314–3319.

Yushmanov, V.E., Mandal, P.K., Liu, Z., Tang, P., and Xu, Y. (2003). NMR structure and backbone dynamics of the extended second transmembrane domain of the human neuronal glycine receptor alpha1 subunit. Biochemistry *42*, 3989–3995.

